Improved Modulated Carrier Control With On-Time Doubler for a Single-Phase Shunt Active Power Filter

Gibong Son, Hye-Jin Kim, *Student Member, IEEE*, and Bo-Hyung Cho, *Fellow, IEEE*

***Abstract*—This paper proposes an improved modulated carrier control with on-time doubler for the single-phase shunt active power filter, which eliminates harmonic and reactive currents drawn by nonlinear loads. This control method directly shapes the line current to be sinusoidal and in phase with the grid voltage by generating a modulated carrier signal with a resettable integrator, comparing the carrier signal to the average line current and making duty ratio doubled. Since the line current compared to the carrier signal is not the peak, but the average value, dc-offset appeared at the conventional control methods based on one-cycle control is effectively addressed. The proposed control technique extirpates the harmonic and reactive currents and solves the dc-offset problem. The operation principle and stability characteristic of the single-phase shunt active power filter with the proposed control method are discussed, and experimental results with laboratory prototype under various load conditions verify its performance.**

***Index Terms*—Harmonic and reactive currents elimination, indirect control, modulated carrier control, nonlinear load, one-cycle control, single-phase shunt active power filter.**

I. Introduction

NONLINEAR loads such as diode rectifiers with a capacitive or inductive load generate harmonic and reactive currents from ac sources and cause low efficiency, low power factor, high total harmonic distortion (THD), and some detrimental disturbances to other devices. Thus, tight regulations (e.g., IEC 61000-3-2, IEC 61000-3-12) on harmonic and reactive currents have been established to suppress the serious harmonic contamination caused by proliferation of nonlinear loads.

To comply with the aforementioned regulations, various research works have been conducted. At the earlier stage, simple passive filters such as parallel, series, and hybrid filters consisting of solely passive elements were employed to improve power factor and selectively compensate harmonic currents [1]–[3]. In spite of merits in cost and simplicity, the passive filters are so intolerant of line variations that resonance between the filter and line impedance may aggravate the harmonic pollution at the grid. Active power factor correction (PFC) schemes have been widely used as well, which build an ideal rectifier presenting an effective resistive load to the grid [4]–[6]. Although active PFC achieves almost unity power factor, it requires higher rating power semiconductor devices since it processes the whole power delivered from the grid to the load.

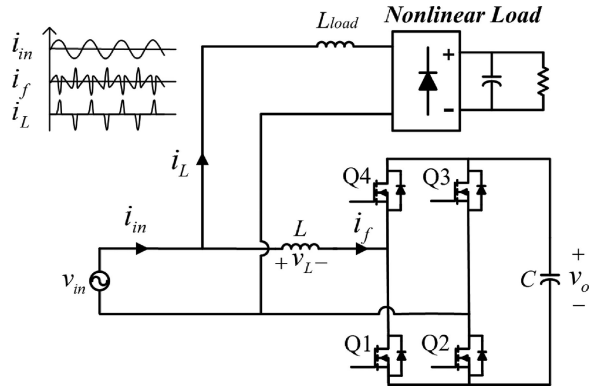

Fig. 1. Single-phase shunt active power filter with nonlinear load.

The other technique, active power filter (APF), has been a reasonable solution to tackle the aforementioned issues. Among a variety of APFs, shunt APF is one of the most practical configurations on account of its simplicity, effectiveness, and versatility. A single-phase shunt APF is connected in parallel with nonlinear loads and compensates the harmonic and reactive components by working as a current source as shown in Fig. 1 so that the line current contains solely the fundamental content of the load current. Based on which current is controlled, the conventional single-phase shunt APF control methods are classified into two groups: 1) direct control method [7]–[10], and 2) indirect control method [11]–[19]. In the direct control method, in order to obtain a reference current for a control converter, the shunt APF, it is necessary to detect the harmonic and reactive elements of the nonlinear load, which means that at least two current sensors are needed to eliminate the unwanted elements in the line current. Furthermore, obtaining the reference current requires precise analog multipliers or high performance processor and A/D modules.

To overcome these drawbacks, the indirect control methods have been introduced, which simply control the line current to follow the grid voltage. The main advantages of this approach are that only one current sensor for the line current is required, and faster transient response is attained. In [11]–[14], the line current reference signal is generated instead of shunt APF current reference by multiplying the grid voltage and the

Manuscript received September 26, 2016; revised November 29, 2016 and January 15, 2017; accepted February 28, 2017. Date of publication March 15, 2017; date of current version November 2, 2017. Recommended for publication by Associate Editor Carlos Alberto Canesin.

G. Son is with the Hyundai Motor Company, Seoul 137938, South Korea (e-mail: crowbulsik@hotmail.com).

H.-J. Kim is the Senior Engineer in the Mechatronics R&D Center, Samsung Electronics, Suwon 16677, South Korea (e-mail: gpwls12@snu.ac.kr).

B.-H. Cho is with the School of Electrical Engineering, Seoul National University, Seoul 13557, South Korea (e-mail: bhcho@snu.ac.kr).

Color versions of one or more of the figures in this paper are available online at http://ieeexplore.ieee.org.

Digital Object Identifier 10.1109/TPEL.2017.2682794

output signal of the dc-link voltage compensator with different combinations or additional functions. Then, the shunt APF operates to drive the line current to pursue the grid voltage. Although these sorts of indirect control compensate unwanted currents properly, they still have calculation burden on the reference generation as the load level changes and need to use the analog multipliers as well.

In contrast, the indirect controls based on one-cycle control [20] do not generate the line current reference but use an integrator with reset as a key component to control the duty ratio of the shunt APF, which drastically simplifies the control circuit without multiplying function [15]–[19]. Nevertheless, because the peak value of the line current is programmed to be compared with the reference signal, dc-offset arises especially at light loads. The dc-offset problem renders power factor and efficiency deteriorated. In [16] and [18], the slope of the carrier signal is modified in the way either an artificial ramp or one more integrator is added to resolve the dc-offset problem, but this compensation leads to increase in the current control loop complexity. Unipolar operation mode alleviates dc-offset since the shunt APF at positive and negative half-cycle operates symmetrically [17]. However, the method complicates the gating logic at each half-cycle of the grid voltage. On top of that, these are relatively susceptible to noise in the sensed line current as both control methods use the peak current to reset a latch.

This paper proposes a new single-phase shunt APF control method using an improved modulated carrier signal and an on-time doubler to solve the dc-offset problem. The slope of the modulated carrier signal is determined for the parallel connection of the nonlinear load and the shunt APF to be a resistive load to the grid. By comparing the carrier signal to the average line current and making the duty ratio doubled, the proposed control technique accomplishes no dc-offset, noise immunity, and good compensation performance as well. In Section II, the operation principle is analyzed in detail, and verification of the proposed control scheme is theoretically proved. In Section III, the small-signal model of the shunt APF system is given to design the voltage controller. Experimental results with a laboratory prototype (1.6-kW nonlinear load with a shunt APF) are provided to validate the performance of the proposed control method in Section IV. Finally, the paper is concluded in Section V.

II. Operation Principle

A. Operation Analysis of Power Stage

The shunt APF with the proposed control method is operated in bipolar mode as illustrated in Fig. 2. At positive half-cycle of the grid voltage, Q1, Q3 are ON and Q2, Q4 are OFF during $0 < t < dT_s$, and Q2, Q4 are ON and Q1, Q3 are OFF during $dT_s < t < T_s$, vice versa at negative half-cycle, where T_s is the switching period, and d is the duty ratio of the converter. Fig. 3(a) and (b) shows the equivalent circuit of the shunt APF system during one switching cycle in which the nonlinear load is expressed as a constant current source i_L.

On the assumption that 1) the switching frequency of the shunt APF f_s is much higher than those of the line and the nonlinear load currents, 2) the capacitance of the dc-link capacitor C is large enough so that v_o is regulated to be a constant value V_o in each switching cycle, the shunt APF current i_f is approximately constant during a switching period. Then, by using volt-second balance of the APF inductor L in the equivalent circuit of the shunt APF shown in Fig. 3

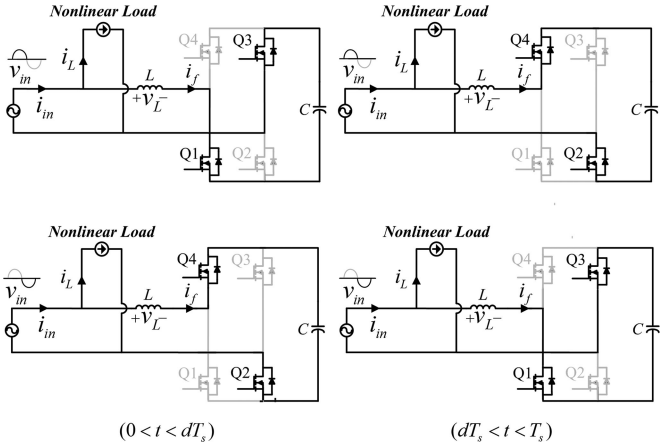

Fig. 2. Operation modes of the shunt APF power stage.

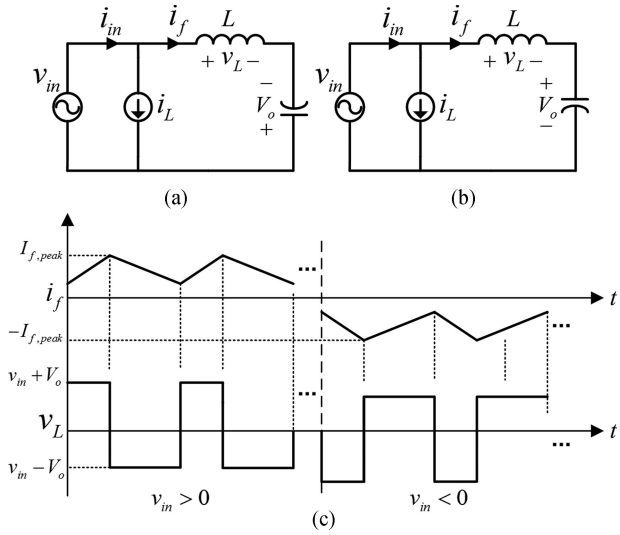

Fig. 3. Equivalent circuit of the shunt APF and operation waveforms. (a) $0 < t < dT_s$ when $v_{\rm in} > 0$, (b) $dT_s < t < T_s$ when $v_{\rm in} > 0$, and (c) APF inductor current and voltage.

$$L\frac{di}{dt} = v_{\rm in} + V_o \ (0 < t < dT_s) \tag{1}$$

$$L\frac{di}{dt} = v_{\rm in} - V_o (dT_s < t < T_s) \tag{2}$$

$$d(v_{\rm in} + V_o) + d'(v_{\rm in} - V_o) = 0. \tag{3}$$

From (1) and (2), (3) is derived, and the relation between the grid voltage $v_{\rm in}$ and the shunt APF's dc-link voltage V_o is given by

$$V_o = \frac{1}{(1-2d)} v_{\rm in}. \tag{4}$$

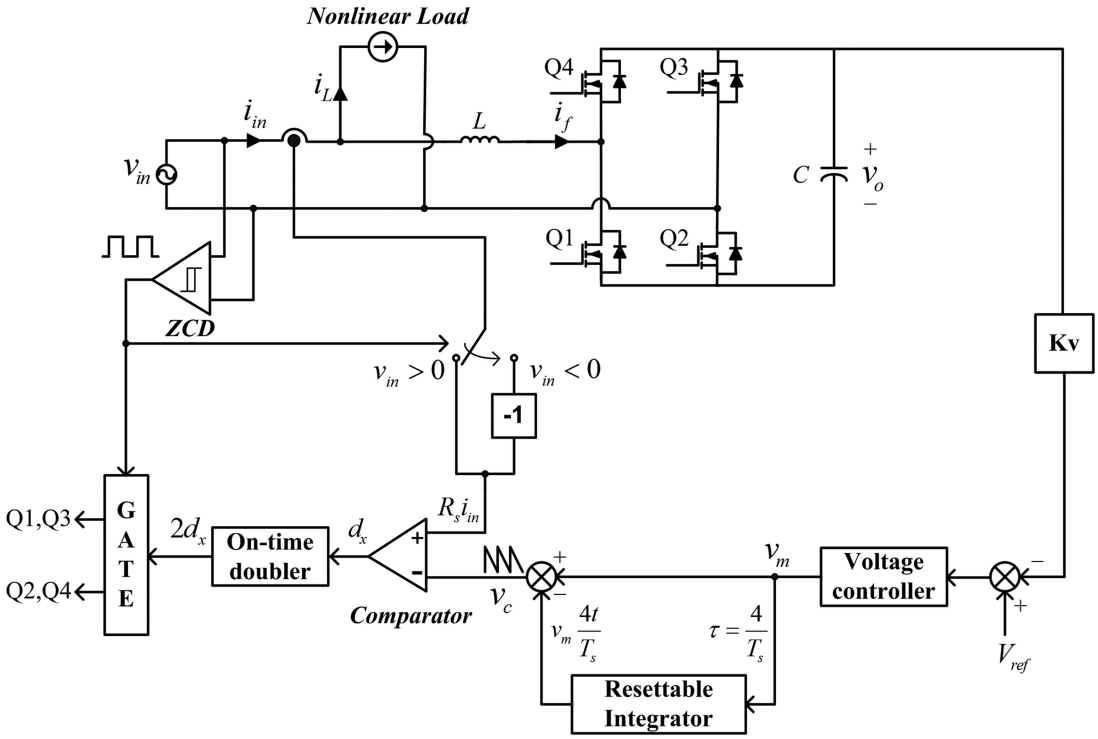

Fig. 4. Overall control structure of the proposed control method with the shunt APF.

B. Proposed Control Scheme

To make the line current follow the grid voltage, following equation must be satisfied that is the key concept of PFC control:

$$\frac{v_{\text{in}}}{i_{\text{in,avg}}} = R_e \tag{5}$$

where $i_{\text{in,avg}}$ is the averaged line current in one switching period and R_e is the constant of proportionality known as the emulated resistance. By combining (4) and (5), the control equation for the proposed control method is presented as

$$R_s i_{\text{in,avg}} = R_s \cdot \frac{V_o}{R_e}(1-2d) = v_m(1-2d) \tag{6}$$

where R_s is the line current sensing gain and v_m is $R_s V_o / R_e$. Then, (5) is realized by controlling d to satisfy (6) in a switching cycle.

Fig. 4 illustrates the proposed control circuit with the shunt APF. In Fig. 4, the nonlinear load current i_L is represented as a current source. The control circuit consists of a voltage controller, a resettable integrator, a comparator, an on-time doubler, a zero crossing detection circuit, and a bidirectional switch for the line current sensing. The sensed dc-link voltage is compared to the reference voltage V_{ref} and the error voltage is fed to the voltage controller. The voltage controller output v_m determines the amplitude of the modulated carrier signal. The modulated carrier signal v_c is generated by integrating v_m with a time constant $\tau = T_s/4$ and subtracting it from v_{m} expressed as

$$v_c(t) = v_m\left(1 - \frac{4t}{T_s}\right) \ (0 < t < T_s). \tag{7}$$

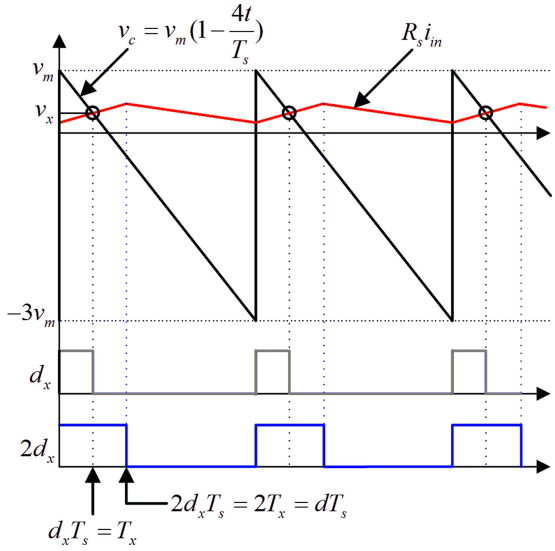

Fig. 5. Duty generation mechanism of the proposed control method.

When the sensed line current $R_s i_{\text{in}}$ reaches the modulated carrier signal v_c, the comparator outputs d_x, and the duration of this signal is processed to be doubled [21]–[23] $2d_x$ by the on-time doubler in Fig. 4. The processed signal d becomes the duty ratio of the shunt APF. As the slope of the sensed line current is uniform during $0 < t < dT_s$, the sensed line current at $t = d_x T_s = T_x$ in Fig. 5 is exactly the average value. Therefore, modifying the duty ratio d as the two-fold of d_x allows v_c to be compared with the average value of the sensed line current which, in turn, guarantees no appearance of the dc-offset problem. Fig. 5 shows the mechanism of the proposed control

method and the following equation is obtained at $t = T_x$:

$$v_x = R_s i_{\text{in,avg}} = v_c(T_x) = v_m\left(1 - \frac{4T_x}{T_s}\right) = v_m(1-2d). \tag{8}$$

Combination of (4) and (8) yields

$$\frac{v_{\text{in}}}{i_{\text{in,avg}}} = R_s\frac{V_o}{v_m} = R_e. \tag{9}$$

It can be inferred from (9) that the average line current is proportional to v_{in} and this allows a unit power factor with the grid voltage. Therefore, parallel connection of the nonlinear load and the shunt APF emulates a resistive load from the viewpoint of the ac source.

C. Stability Analysis of the Proposed Control

Stability characteristic of the current control loop with the proposed control method is examined by observing the change in a perturbation of the line current over one switching period [24]. Fig. 6 depicts the steady-state and perturbed line current waveforms of the shunt APF with the proposed control method where m_1, $-m_2$, $-m_a$, $\hat{i}_L(0)$, $\hat{i}_L(T_s)$, and $\hat{d}$ are the on-time slope of the line current, the off-time slope of the line current, the slope of the improved modulated carrier signal, the initial line current perturbation, the line current perturbation at T_s, and the change in duty ratio caused by the perturbation, respectively. m_1 and $-m_2$ are regarded to be constant assuming that the amount of the line current perturbation is negligibly small which is exaggerated in Fig. 6 for the sake of easy understanding. The line current perturbations at $t = 0, t = T_s$ and correlation between two values are expressed as follows:

$$\hat{i}_L(0) = \left(\frac{m_1}{2} + \frac{m_2}{2}\right)\hat{d}T_s \tag{10}$$

$$\begin{aligned}\hat{i}_L(T_s) &= m_2\hat{d}T_s - \{I_{L0} + \hat{i}_L(0) + m_1(D-\hat{d})T_s \\ &\quad - (I_{L0} + m_1 DT_s)\} \\ &= \left(m_2 + \frac{m_1}{2} - \frac{m_a}{2}\right)\hat{d}T_s \end{aligned}\tag{11}$$

$$\hat{i}_L(T_s) = \frac{2m_2 + m_1 - m_a}{m_1 + m_a}\cdot\hat{i}_L(0) \tag{12}$$

where m_1 is $(v_{\text{in}} + V_o)/L$, m_2 is $(V_o - v_{\text{in}})/L$, and m_a is $4v_m/T_s$. Equation (12) can be extended to the generalized form as expressed in the following:

$$\hat{i}_L(nT_s) = \hat{i}_L(0)\cdot\left(\frac{2m_2 + m_1 - m_a}{m_1 + m_a}\right)^n = \hat{i}_L(0)\cdot\alpha^n \tag{13}$$

where $\hat{i}_L(nT_s)$ is the perturbed line current at nth switching cycle from the initial perturbation, and α is the characteristic value of the line current perturbation. For the control system to be stable, $\hat{i}_L(nT_s)$ must decay to zero as the number of switching

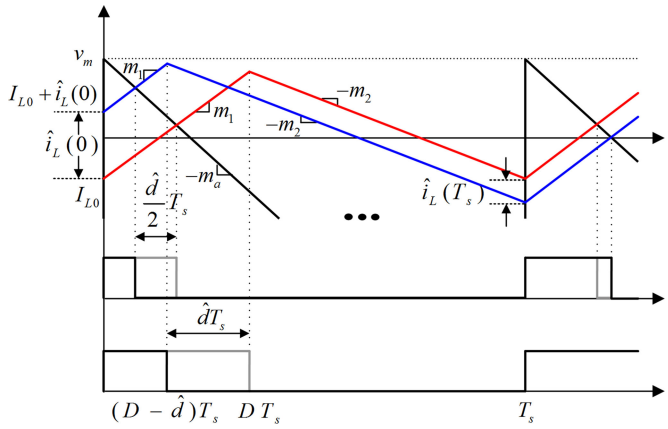

Fig. 6. Steady-state and perturbed line current waveforms.

cycle n increases, that is

$$|\alpha| = \left|\frac{2m_2 + m_1 - m_a}{m_1 + m_a}\right| < 1 \tag{14}$$

$$1 - \frac{v_{\text{in}}}{V_o} < \frac{2Lv_m}{T_s R_s V_o}. \tag{15}$$

Expressing m_1, m_2, and m_a in (14) in terms of v_{in}, V_o, L, v_m, and T_s yields (15) which is the prerequisite for the current control loop stability. Combination of (6) and (15) gives

$$R_e < \frac{2L}{T_s\cdot\left(1 - \frac{v_{\text{in}}}{V_o}\right)}. \tag{16}$$

This is the condition of an emulated resistance when active boost PFC is operating in continuous conduction mode [24], [25]. In other words, the current control loop of the proposed control is stable as long as the shunt APF system operates in CCM because parallel connection of the shunt APF and the nonlinear load seems to be an emulated resistance from the perspective of the grid voltage. As the converter topology used in the paper allows bidirectional power flow, the shunt APF system always operates in CCM and naturally (15) is satisfied. Consequently, with the proposed control method the current control loop stability is guaranteed regardless of the grid voltage, the output voltage, and load conditions and localized subharmonic instability arisen under light load operation is effectively lessened without an external ramp added to the carrier signal [16].

III. Small-Signal Modeling for Voltage Control

To regulate the dc-link capacitor voltage, the voltage controller needs to be designed properly. For such design, small-signal transfer function of control voltage v_m to output voltage v_o must be clarified. This step starts from looking into the large-signal model of the shunt APF system. Power balance technique can derive the large-signal model in a line cycle when assuming that the shunt APF is loss free. The input power is equal to the sum of the output power consumed by the nonlinear load and that handled by the shunt APF [17], that is

$$p_{\text{in}} = \frac{{v_{\text{in}}}^2}{R_e} = p_{\text{out}} = P_{\text{load}} + v_o\cdot i_o \tag{17}$$

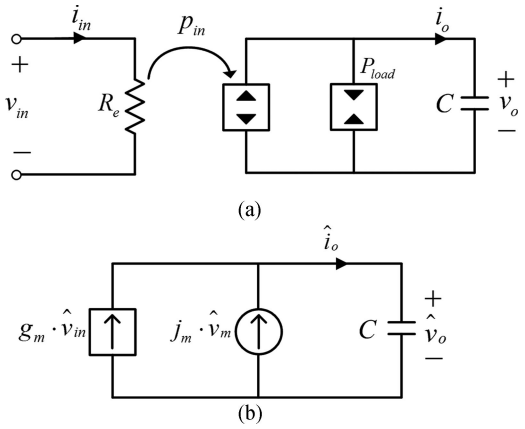

Fig. 7. (a) Large-signal low frequency model of the shunt APF system. (b) Small-signal model of the shunt APF system.

where $p_{\rm in}$ is the instantaneous input power, $p_{\rm out}$ is total power consumed by the shunt APF system, $P_{\rm load}$ is the nonlinear load power, and i_o is the dc-link capacitor current. Substituting (9) into (17) gives the large-signal (18) that represents the overall power flow of the system as shown in Fig. 7(a):

$$\frac{{v_{\rm in}}^2}{R_s \cdot v_o} \cdot v_m = P_{\rm load} + v_o \cdot i_o. \tag{18}$$

To construct the small-signal model, perturbation and linearization process in [24] is used on (18) and the following equation is acquired:

$$\widehat{i_o} = g_m \cdot \widehat{v}_{\rm in} + j_m \cdot \widehat{v}_m - \frac{2}{r_o} \cdot \widehat{v_o} \tag{19}$$

where

$$g_m = \frac{2V_{\rm in} \cdot V_m}{R_s \cdot {V_o}^2} \tag{20}$$

and

$$j_m = \frac{{V_{\rm in}}^2}{R_s \cdot {V_o}^2} \tag{21}$$

and

$$r_o = \frac{V_o}{I_o}. \tag{22}$$

Since it is assumed that the large-signal model is ideal and theoretically the shunt APF does not handle any active power, the dc value of capacitor current I_o is zero. Then, the small-signal resistance r_o becomes infinite, and the small-signal model is simplified as Fig. 7(b). The small-signal transfer function from the capacitor current to the output voltage is expressed as

$$\frac{\widehat{v_o}}{\widehat{i_o}} = \frac{1}{sC}. \tag{23}$$

Finally, the control voltage to the output voltage small-signal transfer function is yielded by combination of (19) and (23):

$$\frac{\widehat{v_o}}{\widehat{v_m}} = j_m \cdot \frac{1}{sC}. \tag{24}$$

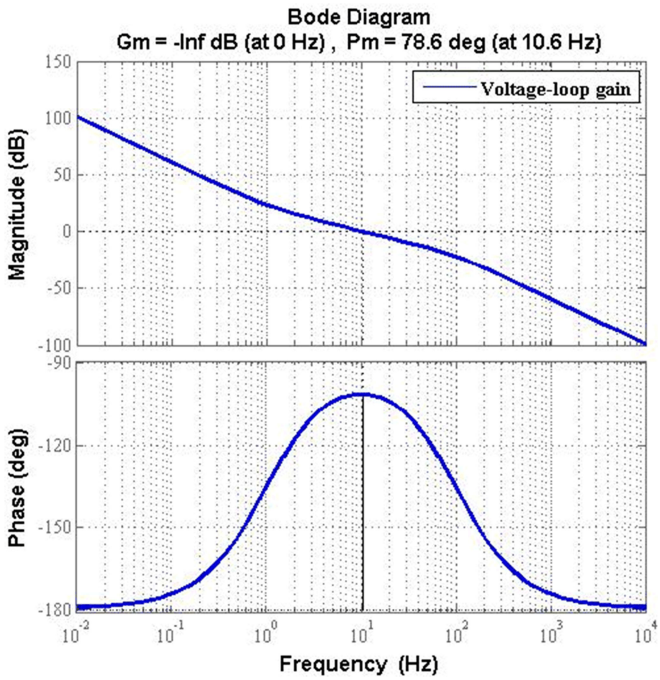

Fig. 8. Bode diagram for voltage-loop gain of the shunt APF system.

TABLE I
SPECIFICATION OF THE PROTOTYPE

Condition	Value
Maximum Load Power ($P_{\rm load}$)	1.6 kW
Grid Voltage ($v_{\rm in}$)	220 Vrms/60 Hz
APF Inductor (L)	1 mH
APF Capacitor (C)	800 μF
DC-link Voltage (v_o)	400 Vdc
Load Inductor ($L_{\rm load}$)	2 mH
Load Capacitor ($C_{\rm load}$)	600 μF
Switching Frequency (f_s)	60 kHz
MOSFET Q1, Q2, Q3, Q4	SIHG20N50C
DSP controller	TMS320F28335

Based on (24), the output voltage compensator $G_v(s)$ is designed as follows:

$$G_v(s) = w_k \frac{\left(1 + \frac{s}{w_z}\right)}{s\left(1 + \frac{s}{w_p}\right)}. \tag{25}$$

The integrator plays a role to remove dc error. The zero is placed at 1 Hz to prevent the slope of the voltage from becoming –40 dB/decade at crossover frequency to assure sufficient phase margin, while the pole is placed at 1 kHz to attenuate the high frequency noise, but not to affect the phase margin. w_k is selected for the voltage loop to have very low bandwidth (approximately 10 Hz) avoiding the line current distortion. With the output voltage compensator, the bode diagram of the shunt APF system's voltage-loop gain is plotted as Fig. 8. System parameters used to design the voltage control loop are specified in Table I. It is expected from Fig. 8 that the dc-link voltage of the shunt APF is stably regulated because the voltage-loop gain has very low crossover frequency (10.6 Hz) and sufficient phase margin (78.6 degree).

IV. Experimental Results

Laboratory prototype of a single-phase shunt APF system with the improved modulated carrier control is implemented to validate the performance of the new control method. The power stage and the control circuit are realized on the basis of Fig. 4. The photograph of the laboratory prototype is shown in Fig. 9 and the specification of the prototype is organized in Table I.

The main element of the control circuit, the modulated carrier signal and the on-time doubler, can be simply realized in two ways. Kim *et al*. [26] introduces an analog method using purely analog circuitry and a hybrid method effectively mixing analog and digital controllers for multiphase interleaved boost PFC. By virtue of its cost effectiveness and implementation flexibility, the hybrid method is applied for the prototype specified in Table I and partially modified to be suitable for the proposed control scheme as depicted in Fig. 10(a). The modulated carrier signal v_c is obtained by integrating the inverted voltage controller output $-v_m$ with reset and subtracting it from the voltage controller output v_m. The comparator outputs high signal when the sensed line current intersects the carrier signal and this set signal triggers an interrupt event in DSP. Once the interrupt event is perceived, the DSP internal counter at the moment (CNT) which is initialized to zero at each switching cycle is captured and processed to be doubled (2CNT). Finally, the calculated DSP internal counter is converted in terms of duty v_{duty}. The operation mechanism of the current controller with this hybrid method is illustrated in Fig. 10(b).

Experimental waveforms of the shunt APF system with the proposed control method are shown in Figs. 11 and 12. Fig. 11 illustrates the grid voltage, the line current, the load current, and the shunt APF current at 220-Vrms under full-load condition (1.6-kW nonlinear load), whereas Fig. 12 shows them under half-load condition (800-W nonlinear load). It can be seen that the line current is almost sinusoidal and in phase with the grid voltage. These figures show that, regardless of how much currents flow to the nonlinear load, the line current contains mostly the fundamental component of the nonlinear load. In addition, as expected, the dc-offset problem totally disappears both under full and half-load conditions due to the inherent characteristic of the proposed control. However, when the load current changes stiffly from peak to zero, the line current is slightly distorted. In Section II, the switching frequency is assumed to be significantly higher than that of line and load so that the load and the APF currents are considered to be constant in a switching cycle. Because these currents vary slightly in the real situation, the line current cannot follow the grid voltage perfectly at the moment the load current drastically changes. If the load current changes slowly in a line cycle, this phenomenon is not observed. Although increasing the switching frequency mitigates the current distortion as well, trade-off between the efficiency of the system and THD needs to be taken account of.

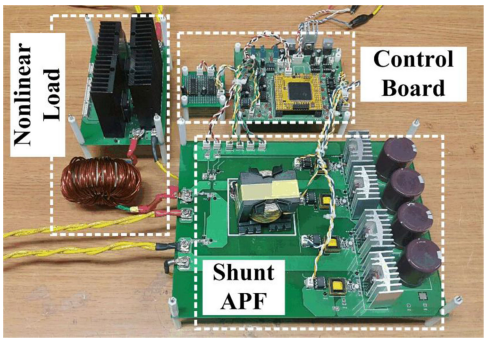

Fig. 9. Laboratory prototype of the 1.6 kW shunt APF system.

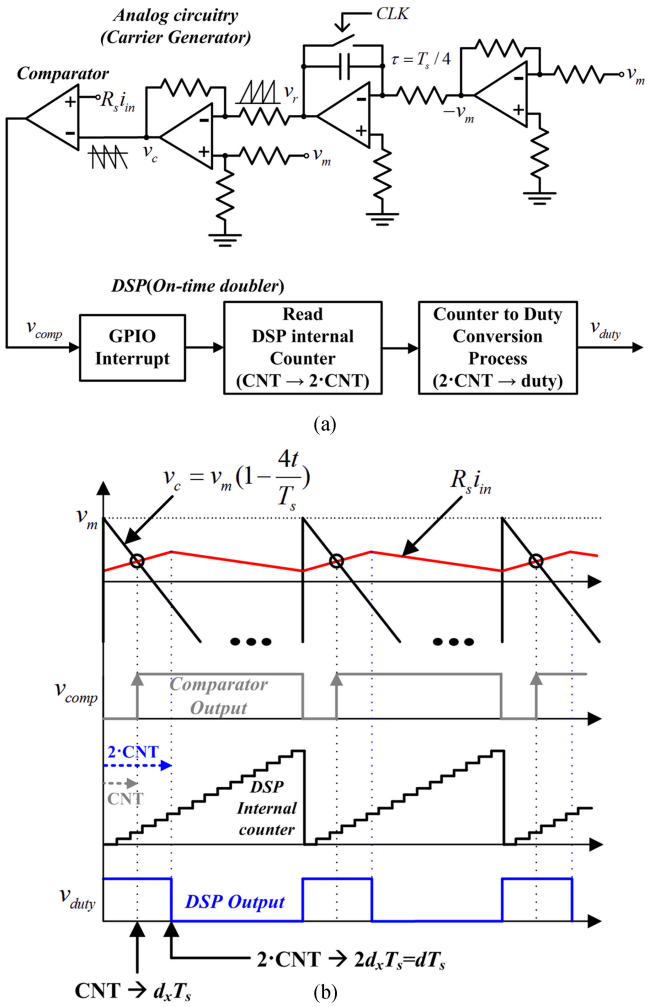

Fig. 10. (a) Current controller implementation using hybrid method. (b) Operation mechanism of the current controller with the hybrid method.

Fig. 13 represents the switching mechanism of the proposed modulated carrier control method which agrees with that depicted in Fig. 10(b). When the sensed line current reaches the carrier signal, the comparator outputs a high signal and duty is generated as two-fold of d_x. This allows the average line current to be compared with the carrier signal as intended. The experimental result of the load transient response is shown in Fig. 14. The load conditions change from half (800 W) to full (1.6 kW). As soon as the load increases, the dc-link voltage is raised to the origin right away, 400 ms, in this system, which suggests that the voltage compensator is appropriately designed. It is implied that the shunt APF system with the proposed modulated carrier control guarantees magnificent performance not

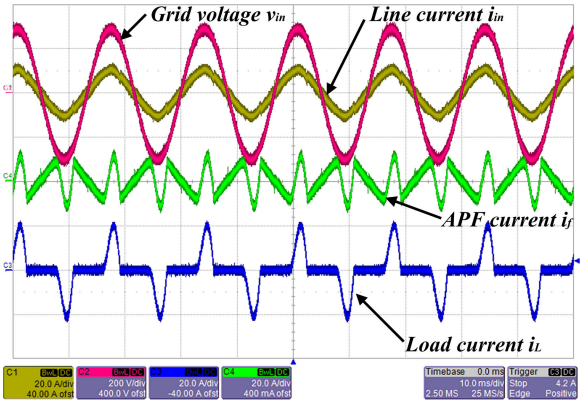

Fig. 11. Measured grid voltage, line current, APF current, and load current waveforms of the shunt APF system based on the proposed control method at full load condition ($v_{\rm in}$ 200 V/div, $i_{\rm in}$ 20 A/div, i_f 20 A/div, i_L 20 A/div).

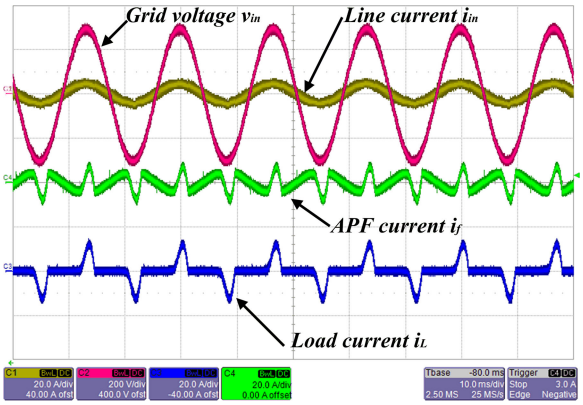

Fig. 12. Measured grid voltage, line current, APF current, and load current waveforms of the shunt APF system based on the proposed control method at half-load condition ($v_{\rm in}$ 200 V/div, $i_{\rm in}$ 20 A/div, i_f 20 A/div, i_L 20 A/div).

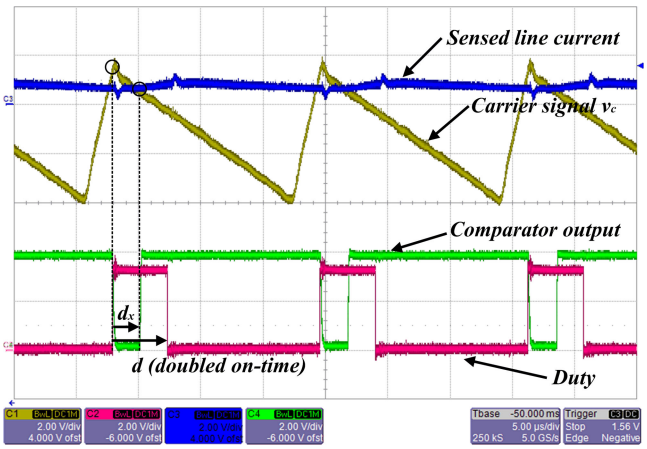

Fig. 13. Current controller switching mechanism.

only in steady state but also in transient state. The experiments at 110 Vrms grid voltage under various load conditions are carried out as well as 220 Vrms as shown in Fig. 15. As expected, the line current has the same shape as the grid voltage and no dc-offset is observed. Nevertheless, the line current distortion

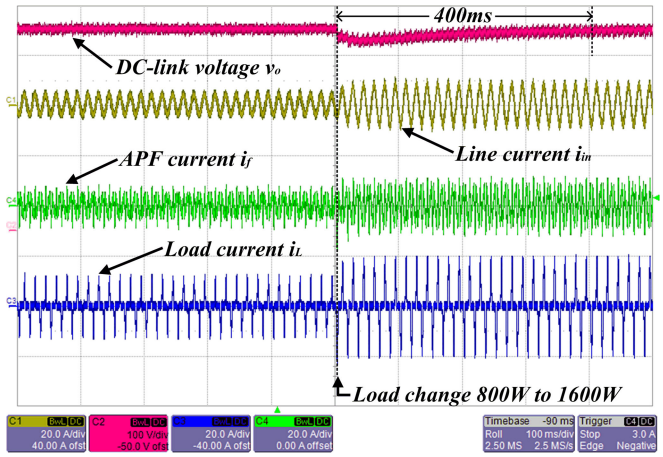

Fig. 14. Measured dc-link voltage, line current, APF current, and load current waveforms of the shunt APF system in load transient from 800 to 1600 W (v_o : 100 V/div, $i_{\rm in}$: 20 A/div, i_f : 20 A/div, i_L : 20 A/div).

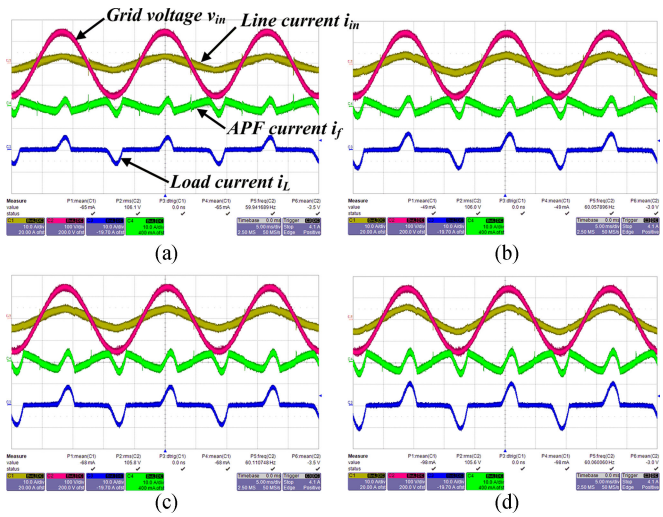

Fig. 15. Measured grid voltage, line current, APF current, and load current waveforms of the shunt APF system at 110 Vrms grid voltage. ($v_{\rm in}$: 100 V/div, $i_{\rm in}$: 10 A/div, i_f : 10 A/div, i_L : 10 A/div.) Under (a) 200 W, (b) 270 W, (c) 340 W, and (d) 400 W load condition.

owing to the abrupt load current change still exists and worsens power factor and THD.

Fig. 16 shows the measured power factor of the shunt APF system with the proposed control method at diverse load conditions. Also, power factor of the nonlinear load system without the shunt APF is represented together. The specific values of both cases are bestowed in Table II. Finally, harmonic elements of the line current with and without the APF under full-load (1.6 kW) condition at 220 Vrms grid voltage are organized in Fig. 17. It is confirmed the system satisfies IEC 61000-3-2 class A with adequate margins. In addition, it is noteworthy mentioning that although the system does not include an input filter for switching ripple attenuation, nearly unit power factor and good harmonic distortion compensation are accomplished (power factor: 0.9891, THD: 8.75% under full-load condition). Further improvement of power factor and THD is expected when

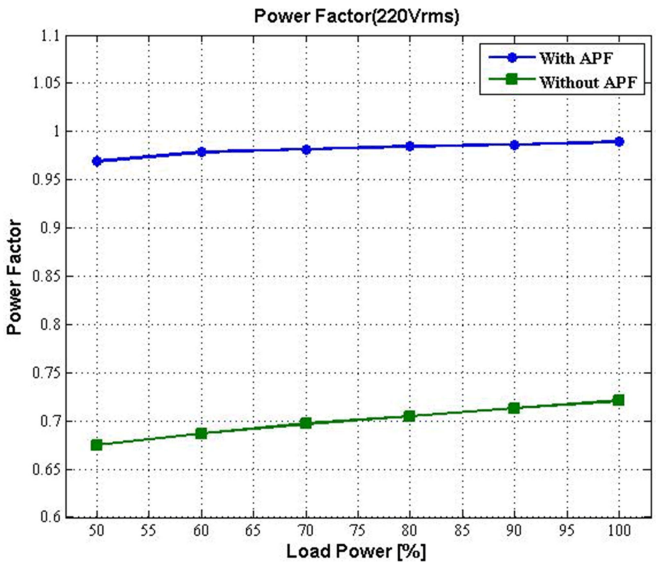

Fig. 16. Power factors of the nonlinear load system with and without the APF under various load conditions.

TABLE II
POWER FACTORS OF THE EXPERIMENT UNDER VARIOUS LOAD CONDITIONS

Condition	50% Load	60% Load	70% Load	80% Load	90% Load	100% Load
W/O APF	0.675	0.687	0.697	0.705	0.713	0.721
W/APF	0.9692	0.9787	0.9816	0.9844	0.9865	0.9891

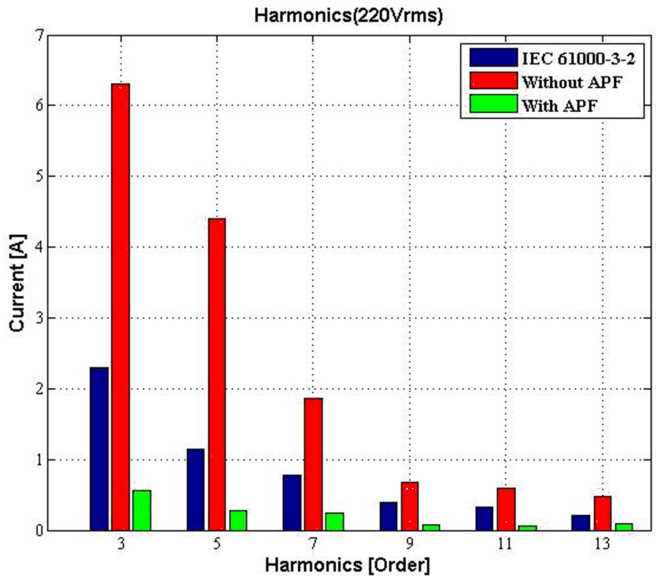

Fig. 17. Harmonic elements of the line current with and without the APF under full load (1.6 kW) condition.

the input filter is added to the system. Data in both Figs. 16 and 17 are collected by a PM-6000 power analyzer.

V. CONCLUSION

An improved modulated carrier control for the single-phase APF has been proposed. The shunt APF with the proposed control method fulfills harmonic and reactive current elimination at the line current by comparing the carrier signal to the average line current and having the duty ratio doubled. On top of that, the control method totally gets rid of the dc-offset problem arisen at the conventional one based on one-cycle control and ameliorates the current control loop stability without additional ramp signal. The operation principle of power stage, the main control mechanism, and the stability characteristic of the current control loop are analyzed in detail. Experimental results with the shunt APF system under assorted conditions verify the performance of the proposed control method in steady and transient states.

REFERENCES

[1] E. B. Makram, E. V. Subramaniam, A. A. Girgis, and R. Catoe, "Hamonic filter design using actual recorded data," *IEEE Trans. Ind. Appl.*, vol. 29, no. 6, pp. 1176–1183, Nov. 1993.
[2] F. Z. Peng, "Harmonic sources and filtering approaches," *IEEE Trans. Ind. Appl. Mag.*, vol. 7, no. 4, pp. 18–25, Jul./Aug. 2001.
[3] L. S. Czarnecki and H. L. Ginn, "The effect of the design method on efficiency of resonant harmonic filters," *IEEE Trans. Power Del.*, vol. 20, no. 1, pp. 286–291, Jan. 2005.
[4] F. A. Huliehel, F. C. Lee, and B. H. Cho, "Small-signal modeling of the single-phase boost high power factor converter with constant frequency control," in *Proc. 23rd Annu. IEEE Power Electron. Spec. Conf.*, vol. 1, 1992, pp. 475–482.
[5] R. Martinez and P. N. Enjeti, "A high-performance single-phase rectifier with input power factor correction," *IEEE Trans. Power Electron.*, vol. 11, no. 2, pp. 311–317, Mar. 1996.
[6] J. R. Pinheiro, H. A. Grundling, D. L. R. Vidor, and J. E. Baggio, "Control strategy of and interleaved boost power factor correction converter," in *Proc. 30th Annu. IEEE Power Electron. Spec. Conf.*, vol. 1, 1999, pp. 137–142.
[7] H.-L. Jou, J.-C. Wu, and H.-Y. Chu, "New single-phase active power filter," *IEE Proc. Electr. Power Appl.*, vol. 141, pp. 129–134, May 1994.
[8] C. Y. Hsu and H. Y. Wu, "A new single-phase active power filter with reduced energy-storage capacity," *IEE Proc. Electr. Power Appl.*, vol. 143, pp. 25–30, Jan. 1996.
[9] L. Zhou and Z. Li, "A novel active power filter based on the least compensation current control method," *IEEE Trans. Power Electron.*, vol. 15, no. 4, pp. 655–659, Jul. 2000.
[10] H. Komurcugil and O. Kukrer, "A New control strategy for single-phase shunt active power filters using a Lyapunov function," *IEEE Trans. Ind. Electron.*, vol. 53, no. 1, pp. 305–312, Feb. 2006.
[11] D. A. Torrey and A. M. A. M. Al-Zamel, "Single-phase active power filters for multiple nonlinear loads," *IEEE Trans. Power Electron.*, vol. 10, no. 3, pp. 263–272, May 1995.
[12] J. -C. Wu and H.-L. Jou, "Simplified control method for the single-phase active power filter," *IEE Proc. Electr. Power Appl.*, vol. 143, pp. 219–224, May 1996.
[13] P. Mattavelli and F. P. Marafao, "Repetitive-based control for selective harmonic compensation in active power filters," *IEEE Trans. Ind. Electron.*, vol. 51, no. 5, pp. 1018–1024, Oct. 2004.
[14] J. Miret, M. Castilla, J. Matas, J. M. Guerrero, and J. C. Vasquez, "Selective harmonic-compensation control for single-phase active power filter with high harmonic rejection," *IEEE Trans. Ind. Electron.*, vol. 56, no. 8, pp. 3117–3127, Aug. 2009.
[15] L. Zhou and K. M. Smedley, "Unified constant-frequency integration control of active power filter," in *Proc. Appl. Power Electron. Conf. Expo.*, 2000, pp. 406–412.
[16] K. M. Smedley, L. Zhou, and C. Qiao, "Unified constant-frequency integration control of active power filters: Steady-stage and dynamics," *IEEE Trans. Power Electron.*, vol. 16, no. 3, pp. 428–436, Jul. 2001.
[17] C. Qiao, K. M. Smedley, and F. Maddaleno, "A single-phase active power filter with one-cycle control under unipolar operation," *IEEE Trans. Circuits Syst.*, vol. 51, no. 8, pp. 1623–1630, Aug. 2004.
[18] Y. Huang, Z. Zhou, and C. Wan, "The modified strategy of active power filter based on one-cycle control," in *Proc. 2008 IEEE Pac.-Asia Workshop Comput. Intell. Ind. Appl.*, 2008, pp. 170–174.

[19] E. S. Sreeraj, E. K. Prejith, K. Chatterjee, and S. Bandyopadhyay, "An active harmonic filter based on one cycle control," *IEEE Trans. Ind. Electron.*, vol. 61, no. 8, pp. 3799–3809, Aug. 2014.
[20] K. M. Smedley and C. Slobodan, "One-cycle control of switching converters," in *Proc. 22nd Annu. IEEE Power Electron. Spec. Conf.*, 1991, pp. 888–896.
[21] H. Choi, "Continuous conduction mode power factor correction circuit with reduced sensing requirement," U.S. patent US8 279 630, Oct. 2, 2012.
[22] H.-J. Kim, B.-H. Cho, and H. Choi, "Interleaved continuous conduction mode power factor correction boost converter with improved modulated carrier control method," in *Proc. Appl. Power Electron. Conf. Expo.*, 2013, pp. 351–355.
[23] G. Son, H.-J. Kim, and B.-H. Cho, "A single-phase shunt active power filter with an improved modulated carrier control," in *Proc. Appl. Power Electron. Conf. Expo.*, 2014, pp. 983–988.
[24] R. W. Erickson and D. Maksimovic, *Fundamental of Power Electronics*. New York, NY, USA: Springer-Verlag, 2001.
[25] H. Kim, B.-H. Cho, and H. Choi, "An improved modulated carrier control of single-phase boost PFC converter," in *Proc. Int. Power Electron. Conf.*, 2014, pp. 2575–2579.
[26] H.-J. Kim, G.-S. Seo, B.-H. Cho, and H. Choi, " A simple average current control with on-time doubler for multiphase CCM PFC converter," *IEEE Trans. Power Electron.*, vol. 30, no. 3, pp. 1683–1693, Mar. 2015.

Gibong Son received the B.S. degree from the Pusan National University, Pusan, South Korea, in 2012, and the M.S. degree from the Seoul National University, Seoul, South Korea, in 2014, both in electrical engineering.

He has been working with Hyundai Motor Company, Seoul, South Korea, since 2014. His research interests include power electronics in electric vehicle, power factor correction converter, and resonant converters.

Hye-Jin Kim (S'12) received the B.S., M.S., and Ph.D. degrees in electrical engineering from the Seoul National University, Seoul, South Korea, in 2010, 2012, and 2016, respectively.

Since 2016, he has been a Senior Engineer in the Mechatronics R&D Center, Samsung Electronics, Suwon, South Korea. His research interests include design, analysis, and control of power factor correction converters and distributed power systems, and high voltage applications.

Bo-Hyung Cho (M'89–SM'95–F'11) received the B.S. and M.S. degrees from the California Institute of Technology, Pasadena, CA, USA, in 1978 and 1980, respectively, and the Ph.D. degree from the Virginia Polytechnic Institute and State University (Virginia Tech), Blacksburg, VA, USA, in 1985, all in electrical engineering.

Prior to his research at Virginia Tech, he was a member of the Technical Staff with the Department of Power Conversion Electronics, TRW Defense and Space System Group, USA. From 1982 to 1995, he was a Professor in the Department of Electrical Engineering, Virginia Tech. In 1995, he joined the School of Electrical Engineering, Seoul National University, Seoul, South Korea, where he is currently a Professor. His current research interests include power electronics, modeling, analysis, and control of spacecraft power processing equipment, and distributed power systems.

Dr. Cho is a member of Tau Beta Pi. He received the 1989 Presidential Young Investigator Award from the National Science Foundation. He chaired the 2006 IEEE Power Electronics Specialists Conference.